Transport and interaction blockade of cold bosonic atoms in a triple-well potential

2010 New J. Phys. 12 065020

(http://iopscience.iop.org/1367-2630/12/6/065020)

New Journal of Physics
The open-access journal for physics

Transport and interaction blockade of cold bosonic atoms in a triple-well potential

P Schlagheck[1,2,3], **F Malet**[1], **J C Cremon**[1] **and S M Reimann**[1,3]
[1] Mathematical Physics, LTH, Lund University, Box 118, 22100 Lund, Sweden
[2] Département de Physique, Université de Liège, 4000 Liège, Belgium
E-mail: Peter.Schlagheck@ulg.ac.be and stephanie.reimann@matfys.lth.se

New Journal of Physics **12** (2010) 065020 (16pp)
Received 29 November 2009
Published 28 June 2010
Online at http://www.njp.org/
doi:10.1088/1367-2630/12/6/065020

Abstract. We theoretically investigate the transport properties of cold bosonic atoms in a quasi-one-dimensional (1D) triple-well potential that consists of two large outer wells, which act as microscopic source and drain reservoirs, and a small inner well, which represents a quantum-dot-like scattering region. Bias and gate 'voltages' introduce a time-dependent tilt of the triple-well configuration, and are used to shift the energetic level of the inner well with respect to the outer ones. By means of exact diagonalization considering a total number of six atoms in the triple-well potential, we find diamond-like structures for the occurrence of single-atom transport in the parameter space spanned by the bias and gate voltages. We discuss the analogy with Coulomb blockade in electronic quantum dots, and point out how one can infer the interaction energy in the central well from the distance between the diamonds.

Contents

[3] Authors to whom any correspondence should be addressed.

1. Introduction

The development of quasi-one-dimensional (1D) waveguides for cold atoms based on optical lattices [1] and atom chips [2, 3] has led to a number of theoretical investigations on the guided quasi-stationary and dynamical transport properties of ultracold atomic gases [4–9]. Particular attention was devoted to the transport of coherent bosonic matter waves through quantum-dot potentials realized, e.g., by two (magnetic or optical) barriers along the waveguide, which display nonlinear transmission features that are reminiscent of nonlinear optics [6–10]. An important long-term aim in this context is to establish a close analogy with *electronic* conduction through microfabricated structures and nanostructures in solid-state systems. This latter field of research still exhibits a number of open questions, especially related to the quantitative role of interaction and correlation between the electrons in such mesoscopic transport processes.

In spite of remarkable advancements in the creation of 1D matter-wave beams through guided atom lasers [11, 12], the experimental realization and evaluation of such 1D atomic scattering processes still represents a formidable task. It therefore makes sense to consider alternative approaches based on *closed* systems, where two reservoirs of ultracold atoms are connected to each other and biased such that a flow of atoms can take place from one reservoir to the other. Atomic quantum dots across which the atoms have to tunnel could be implemented by inducing small potential wells in between the reservoirs. Such geometries were studied in recent investigations on transistor-like operations with Bose–Einstein condensates [13]. The quantification of 'conduction' across such a quantum dot under a small bias, however, requires a precise measurement of atomic populations ideally on a single-atom level, which is not impossible [14] but seems rather hard to be achieve in this specific context.

A solution to the problem of counting individual atoms was recently provided by experiments with optical double-well lattices, focusing on correlated two-particle tunneling [15] as well as on the interaction blockade [16] with three particles [17]. In these experiments, each double-well site was identically prepared with a well-defined number of atoms and finally 'read out' by absorption imaging after time-of-flight expansion, where the populations in the left and right wells were, before switching off the lattices, transferred to different Brillouin zones. This parallel processing of identical few-particle experiments especially allowed for the detection of integer atomic populations in each of the two wells per site [17], as a consequence of the strong repulsive interaction between the atoms. More recently, much theoretical work has focused on the tunneling of bosons in such double well potentials (see, for example, [18–22]).

Inspired by the basic idea sketched above, we now propose here to investigate source–drain transport processes with ultracold atoms on the basis of optical *triple-well* lattices, which could possibly be realized by adding another standing-wave beam with the appropriate wavelength to the experimental setup in [15, 17]. If all three lattice potentials that together form the triple-well lattice are imposed with about the same amplitude and with a suitable phase shift relative to each other, a triple-well potential can be created on each site where the two outer wells are considerably larger than the inner one. After loading the lattice with a well-defined number of atoms per site, these outer wells can be regarded as microscopic 'source' and 'drain' reservoirs, while the central well acts as an atomic quantum dot.

We now use this general configuration in this paper in order to study the atomic analogue of *Coulomb blockade* in electron transport (see, for example, [23–27] and the review [28])

in the conduction of strongly interacting bosonic atoms from the source to the drain across the dot region. We consider, to this end, a time-dependent ramping process of a bias between the outer wells, which can be implemented by varying the amplitude and phase of the main (longest-wavelength) component of the triple-well lattice, and address the question of to what extent this ramping process leads to the transfer of one or several atoms from the source reservoir to the dot, or from there to the drain reservoir. While this perturbation represents the analogue of a 'bias voltage' in electronic quantum dots, a 'gate voltage', which lowers the on-site eigenenergies of the central well relative to the outer ones, can be induced in a very similar manner, again by a suitable manipulation of the main laser beam of the lattice. Our aim is to map out the lines of finite 'conductance', i.e. of a finite transfer of atoms between the wells, in the parameter space spanned by the above-mentioned gate and bias voltages. We shall show that this gives rise to diamond-like structures that are closely analogous to Coulomb diamonds in electronic quantum dots.

We start in section 2 with a detailed description of the triple-well system under consideration, which is defined in accordance with the experimental setups used in [15, 17]. Section 3 is devoted to the discussion of the 'static' interaction blockade in the triple-well system in perfect analogy with the double-well interaction blockade experiment in [17]. In section 4, we discuss the outcome of the time-dependent ramping process, which is numerically computed both through diagonalization of the many-body Hamiltonian and through the propagation of the many-body wavefunction under the variation of the bias. The resulting diamond structures are explained within a simple Bose–Hubbard model and compared with electronic Coulomb diamonds. We finally discuss the relevant energy scales of this transport process and point out possible implications for future research in the Conclusion.

2. The setup

We consider a gas of ultracold ^{87}Rb atoms in a quasi-1D confinement that is exposed to a periodic potential of the form

$$V(x) = V_0(-\cos kx + \cos 2kx - \cos 4kx) - V_g \cos kx - V_b \sin kx. \tag{1}$$

This potential can be generated by a superposition of three counterpropagating laser beams with the wavelengths $\lambda_1 = 4\pi/k$, $\lambda_2 = 2\pi/k$ and $\lambda_3 = \pi/k$. We specifically consider the wavelengths $\lambda_1 = 1530\,\mathrm{nm}$ and $\lambda_2 = 765\,\mathrm{nm}$, which were also used in the experiments of [15, 17], and assume for the third laser beam the wavelength $\lambda_3 = 382.5\,\mathrm{nm}$. The latter could possibly be realized by a frequency-doubling of the laser beam with the wavelength λ_2 or, alternatively, by retro-reflecting a part of this laser beam (split with an acousto-optical deflector) under a finite angle of 60°, as done in [29]. Using suitable phase shifts between these three counterpropagating laser beams (and taking into account the fact that the wavelength λ_1 is red-detuned, while the wavelengths λ_2 and λ_3 are blue-detuned with respect to the intra-atomic transition in ^{87}Rb), we thereby obtain the effective potential $V_{\mathrm{eff}}(x) = -2V_1 \cos^2(\frac{1}{2}kx - \phi/2) + 2V_2 \cos^2(kx) + 2V_3 \cos^2(2kx - \pi/2)$ with positive prefactors V_1, V_2 and V_3, which apart from a constant offset is exactly equivalent to equation (1), provided we choose $V_1 \cos\phi = V_0 + V_g$, $V_1 \sin\phi = V_b$ and $V_2 = V_3 = V_0$. In this way, we obtain, as shown in figure 1, a periodic lattice of sites with triple-well potentials, where on each site the two outer wells are deeper than the central well.

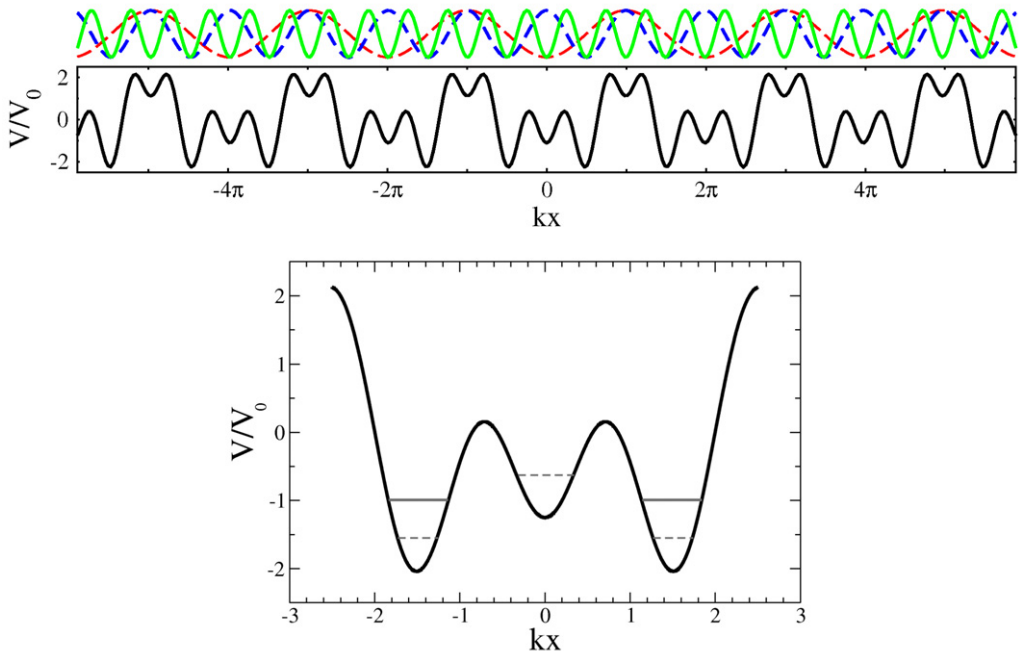

Figure 1. Three optical lattices with the commensurate periods $2\pi/k$, $4\pi/k$ and $8\pi/k$ (upper panel) superimposed according to equation (1) to form a superlattice (middle panel). The lower panel displays the resulting triple-well potential on an individual site of the superlattice (for $V_g = V_b = 0$). The dashed lines mark the unperturbed single-particle energies in the wells, and the solid lines indicate the chemical potential or, more precisely, the particle-removal energy of an individual atom for the six-particle ground state where three atoms are localized in the left as well as in the right well.

The confinement to one spatial direction is assumed to be ensured by the presence of a strong 2D (red-detuned) optical lattice in the transverse spatial directions, described by the effective potential $V_{tr}(y, z) = -V_\perp(\cos k_\perp y + \cos k_\perp z)^2$. This gives rise to a lattice of harmonic waveguides parallel to the x-axis with the confinement frequency $\omega_\perp = 2k_\perp\sqrt{V_\perp/m}$, where m denotes the mass of a ^{87}Rb atom. As was shown by Olshanii [30], the effective 1D interaction strength along these waveguides is given by

$$g = \frac{2\hbar\omega_\perp a_s}{1 - Ca_s/a_\perp}, \tag{2}$$

with $C \simeq 1.4603$, where $a_s \simeq 5.8\,\text{nm}$ is the s-wave scattering length for ^{87}Rb atoms and $a_\perp \equiv \sqrt{\hbar/(m\omega_\perp)}$ denotes the transverse oscillator length. Obviously, a rather large value for $V_\perp$ is generally required in order to induce strong interactions along the 1D confinement. Setting, as in the experiments of [15, 17], the wavelength of the transverse laser beams to $\lambda_\perp \equiv 2\pi/k_\perp = 843\,\text{nm}$, we obtain the 1D interaction strength $g = 4\hbar^2 k/m$ if we choose $V_\perp = 690E_r^\perp$ with $E_r^\perp \equiv \hbar^2 k_\perp^2/(2m)$ being the transverse recoil energy.

We shall in the following consider also a large amplitude of the longitudinal triple-well lattice and set, for the sake of definiteness, the prefactor V_0 in equation (1) to $V_0 = 20\hbar^2 k^2/m = 40E_r$ where $E_r \equiv \hbar^2 k^2/(2m)$ (corresponding to $\simeq$7.8 kHz) is the recoil energy of the laser with

the wavelength λ_2. For this particular choice of the lattice strength, and for $V_b = V_g = 0$, the energetically lowest single-particle eigenstates within each triple-well site are strongly localized in the wells. A rather small splitting $\delta E_{LR} \simeq 0.02\hbar^2k^2/m$ of the ground-state doublet, consisting of the positive and negative linear combinations of the 'Wannier states' (or quasi-modes) in which the atom is localized around the center of the left and right wells, respectively, is thereby obtained, corresponding to a tunneling time scale of the order of $\tau \sim \hbar/\delta E_{LR} \simeq 1$ ms. This splitting is much smaller than the level spacing between the ground-state doublet and the doublet containing an excited state in one of the wells, which is roughly characterized by the local harmonic-oscillator energy $\hbar\omega_{||} \simeq 4\hbar k\sqrt{V_0/m} \simeq 18\hbar^2k^2/m$ within the well. Tunneling between sites of *adjacent* triple wells is neglected in the following, as the associated inter-site tunneling time exceeds all other relevant time scales of this system. We therefore consider the dynamics within the individual triple-well sites to be completely independent of each other.

In addition to the 'main' triple-well lattice characterized by the amplitude V_0, we introduce in equation (1) two independent perturbations with the amplitudes V_g and V_b, which can be controlled by a suitable manipulation of the laser beam with the largest wavelength λ_1. In close analogy with Coulomb blockade experiments in electronic quantum dots, we name V_g the 'gate voltage' and V_b the 'bias voltage'. Indeed, as for electronic quantum dots, the effect of increasing V_g is to lower the energetic offset of the central well with respect to the outer ones, which allows one to enhance the ground-state population of this well in the many-body system. A positive bias voltage V_b, on the other hand, gives rise to an overall tilt of the triple-well configuration, which opens the possibility for a transfer of individual atoms from the left to the central or from the central to the right well.

In lowest order, the impact of the gate and bias voltages V_g and V_b can approximately be quantified by the shifts $E_L \to E_L + V_b$, $E_C \to E_C - V_g$, and $E_R \to E_R - V_b$, of the single-particle energies E_L, E_C and E_R in the left, central and right wells, respectively. This result is obtained by a simple perturbative consideration where the matrix elements of the gate and bias perturbations in equation (1) are evaluated within the local ground states in the wells, which are approximated by Gaussian wavefunctions centered around $kx = 0$ for the central well and around $kx = \pm\pi/2$ for the right and left wells. Using $\omega_{||} \simeq 4k\sqrt{V_0/m}$ as the local oscillator frequency and $V_0 = 20\hbar^2k^2/m$, we obtain $E_{L/R} \to E_{L/R} \pm 0.986V_b$ and $E_C \to E_C - 0.986V_g$. This implies that the gate and bias 'voltages' directly correspond here to the associated energy shifts in the individual wells.

3. Interaction blockade in the ground-state populations

As in [17], we assume that the superlattice is initially loaded with an ultracold gas of ^{87}Rb atoms, such that each of the triple-well sites is populated with a given well-defined number of atoms. In the experiment of [17] that used a double-well lattice, interaction blockade was measured by detecting the ground-state populations in the left and right wells as a function of a finite bias between the wells. For this purpose, the population in the left well was transferred into a highly excited state within the double-well potential by means of a rather fast increase in the bias. This allows one to separately detect it through time-of-flight expansion and subsequent absorption imaging after switching off the optical lattices (see also [15]). A step-like structure, with plateaus at integer values, was found for the population in the left and right wells as a function of the bias [17], which is a clear consequence of the strong repulsive interaction between the atoms.

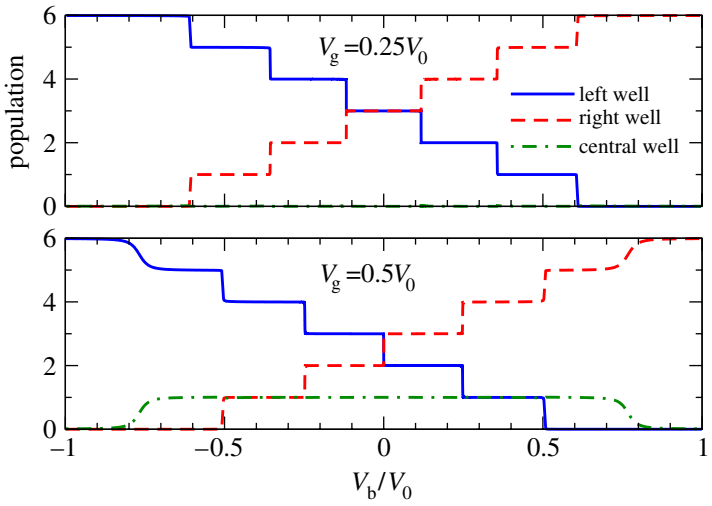

Figure 2. Populations in the left (solid blue line), right (dashed red line) and central wells (dot-dashed green line) for the exact ground state of six particles in the triple-well potential as a function of the bias voltage V_b. The calculation was done for the gate voltages $V_g = 0.25V_0$ (upper panel), for which the central well is practically empty, and for $V_g = 0.5V_0$ (lower panel), for which the central well contains one atom at not too strong bias. Due to the strong repulsive interaction between the atoms, the populations in the wells undergo step-like transitions between plateaus at integer values under the variation of the potential, in close analogy with interaction blockade in double-well lattices [17].

This program can be carried out also for our triple-well configuration. Figure 2 shows, as a function of the bias voltage V_b, the populations in the left, central and right wells that are contained in the many-body ground state of six particles per triple-well site. As in [17], the populations undergo rather sharp, step-like transitions between plateaus at integer values, which clearly underlines the relevance of the strong repulsive interaction between the atoms. While the central well remains practically empty at the gate voltage $V_g = 5$, it is populated with one atom at $V_g = 10$ provided the bias is not too strong. This scenario can straightforwardly be generalized to stronger gate voltages that would allow for two or more atoms in the central well. Decreasing the interaction strength will lead to a decrease in the bias voltage interval in which the sequence of transitions takes place, until in the limit of vanishing interaction this sequence shrinks down to a collective transition from a fully left-biased state, with all atoms in the left well, at negative to a fully right-biased state at positive bias voltages. An infinitely large interaction strength, g, will, on the other hand, not give rise to an infinite interaction energy within the wells and to an infinite extent of the plateaus, but rather approach the case of noninteracting spinless *fermionic* atoms [30] where the Pauli exclusion principle is responsible for the appearance of plateaus and step-like transitions in the populations.

The many-body ground states were calculated by means of an exact diagonalization approach based on the Lanczos algorithm [31], which takes into account all Fock states with a given total number of particles that are defined upon a suitably truncated single-particle basis. We chose as basis functions the plane waves $\phi_n(x) = \sqrt{k/(2\pi)}e^{inkx}$ that satisfy periodic boundary conditions within the triple-well lattice, and took into account for the many-body

calculation all ϕ_n with $-10 \leqslant n \leqslant 10$. We verified that for six particles this truncation is sufficient to reproduce all relevant features of the many-body states under consideration. After calculating the ground state and its many-body eigenfunction, the populations in the individual wells are computed by integrating the spatial atomic density in between (artificial) separation points at the local maxima of the triple-well potential. The population in the left well is thus obtained as the integral over the density from $x = -\pi/k$ to the position of the left local maximum (at $x \simeq -0.7/k$ for $V_g = V_b = 0$), while the population in the central well is given by the integral over the density in between the left and right maxima.

With few exceptions (occurring notably at near-degeneracies between the energies of different many-body states), we almost always obtain nearly integer well populations for the eigenstates, due to the strong repulsive interaction between the atoms. We shall therefore denote these eigenstates by $N_L : N_C : N_R$ in the following, where the integers N_L, N_C and N_R represent the populations in the left, central and right wells, respectively.

4. Interaction blockade in the transport

4.1. Time-dependent ramping process

In contrast to the double-well potential, the confinement (1) permits us to probe interaction blockade not only in the 'static' properties of the many-body ground state, but also in the dynamical *transport* behaviour of the system under the variation of the bias. We assume for this purpose that the triple-well lattice is initially loaded with a given number of atoms at a given gate voltage V_g and at vanishing bias $V_b = 0$. The bias voltage is then *dynamically ramped* from zero to a given maximal value on a suitable time scale. After this ramping process, the population in the individual wells is measured by a suitable transfer of the atoms to excited modes, time-of-flight expansion and absorption imaging [15].

The speed of this ramping has to be chosen such that it is slow with respect to the tunneling time scale between adjacent wells (i.e. between the left and central wells or between the central and right wells), but fast with respect to 'direct' tunneling between the left and right wells. More quantitatively, considering a linear ramping process of the form $V_b(t) = st$ with constant speed s, and taking into account that the shift of the single-particle energy in the left or right wells with respect to the central well is approximately given by V_b (as pointed out in section 2), the Landau–Zener theory for nonadiabatic transitions [32] predicts the probability

$$P = \exp[-2\pi \Delta E^2/(\hbar s)] \tag{3}$$

for the transfer of an atom at an avoided crossing between the state $N_L : N_C : N_R$ and the state $N_L \pm 1 : N_C \mp 1 : N_R$ (or $N_L : N_C \pm 1 : N_R \mp 1$), where ΔE denotes the level splitting between the hybridized states right at the anticrossing. If we denote by δE the analogous level splitting between $N_L : N_C : N_R$ and $N_L \pm 1 : N_C : N_R \mp 1$, corresponding to the transfer of an atom across both barriers, we obtain the requirement that the speed s of the ramping process would have to satisfy $\delta E^2 \ll \hbar s < \Delta E^2$.

In the spirit of this consideration, the outcome of this time-dependent ramping process can be predicted by computing not only the ground state but also lowly excited states of the many-body system as a function of the bias voltage. The lower panel in figure 3 shows the result of such a numerical calculation, which was done for six particles at the gate voltage $V_g = 0.25V_0$. In accordance with figure 2, we recognize that the state with the populations 3:0:3, which is

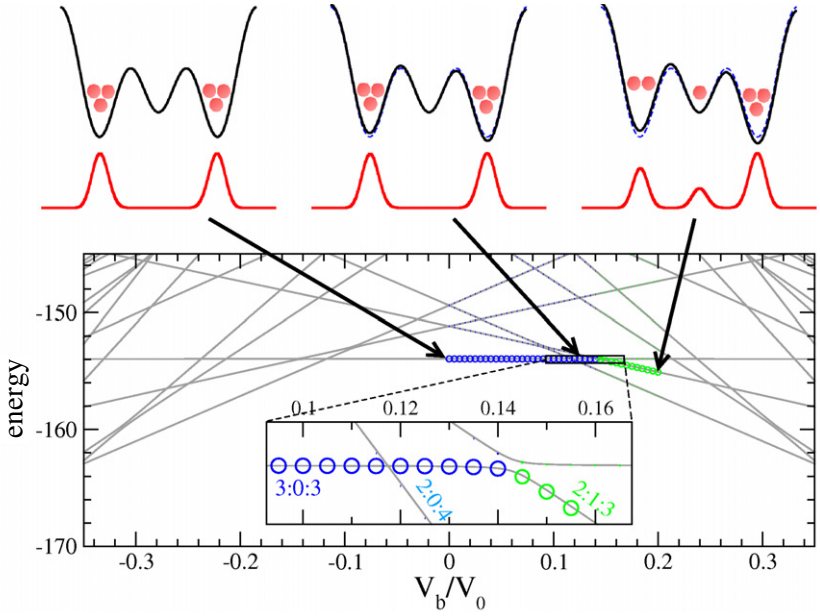

Figure 3. Time-dependent transport process for six particles in the triple-well potential. We start here from an unbiased configuration at gate voltage $V_g = 0.25V_0$ (upper left panel), which is then exposed to a time-dependent sweep of the bias voltage from $V_b = 0$ to $V_b = 0.2V_0$ with the constant speed $dV_b/dt = 0.002\hbar^3k^4/m^2$. The upper panels show the potential (above, in black) and the spatial atom densities (below, in red) for the bias voltages $V_b = 0$ (left panel), $V_b = 0.125V_0$ (middle panel) and $V_b = 0.2V_0$ (right panel). The lower panel illustrates the evolution of this time-dependent ramping process in the many-body spectrum (energies are in units of $\hbar^2k^2/m$). We compute for this purpose the decomposition of the time-dependent many-body wavefunction into the instantaneous eigenstates of the Hamiltonian and represent the relative weight of this decomposition by the size of the circles. Clearly, the system undergoes a nearly perfect transition from the 3:0:3 to the 2:1:3 state at the avoided crossing at $V_b \simeq 0.143V_0$, and is nearly not affected by the previous anticrossing between the 3:0:3 and 2:0:4 states at $V_b \simeq 0.117V_0$.

the energetically lowest state at zero bias, undergoes a small anticrossing with the 2:0:4 state at $V_b \simeq 0.117V_0$, which then represents the new ground state beyond that value of the bias voltage. The level splitting at this anticrossing is found to be $\delta E \simeq 0.001\hbar^2k^2/m$, which is much smaller than the subsequent splitting $\Delta E \simeq 0.069\hbar^2k^2/m$ between the levels of the 3:0:3 and the 2:1:3 states. Consequently, a ramping process $V(t) = st$ with, e.g., the constant speed $s = 0.002\hbar^3k^4/m^2$, altogether taking place within a time interval of $\tau \simeq 0.2V_0/s \simeq 40$ ms, will provide the desired atom transfer from the left to the central well.

This is indeed confirmed by a truly time-dependent simulation of the ramping process. We use for this purpose a variant of the Lanczos algorithm [33], which involves the creation of a finite Krylov subspace that contains the most relevant components describing the time derivative of the wavefunction to be propagated. Within short time intervals δt, a numerically precise propagation is carried out in this Krylov subspace, utilizing the representation of both the

unperturbed part of the Hamiltonian and the time-dependent perturbation within this subspace[4]. In between those time intervals, the Krylov subspace is recreated using the 'new' wavefunction that results from this propagation step. In practice, we find good convergence using 100 Krylov vectors and the time step $\delta t = 1.0\, m/(\hbar k^2)$.

The lower panel of figure 3 shows the result of such a time-dependent calculation for a ramping process of the bias voltage with the speed $s = 0.002\hbar^3 k^4/m^2$ from $V_\mathrm{b} = 0$ to $V_b = 0.2V_0$. To illustrate the evolution in the many-body spectrum, we compute here at regular intervals in time the overlap matrix elements of the wavefunction with the instantaneous eigenstates of the Hamiltonian. This decomposition is then represented in figure 3 by circles whose sizes are directly proportional to the square moduli of those matrix elements. We basically see that the time-dependent wavefunction is, at almost all considered bias voltages, essentially described by one single eigenstate of the Hamiltonian, namely the one that exhibits the populations 3:0:3 before and 2:1:3 after the avoided crossing at $V_\mathrm{b} \simeq 0.143V_0$. The small anticrossing between the 3:0:3 and 2:0:4 states at $V_\mathrm{b} \simeq 0.117V_0$, on the other hand, is almost completely 'ignored' by the time-dependent wavefunction, which undergoes a *diabatic* transition across this anticrossing (in contrast to the adiabatic transition at $V_\mathrm{b} \simeq 0.143V_0$).

This calculation can be carried out for other gate voltages as well. Figure 4 shows, as a function of V_g, the minimal (positive and negative) bias voltages V_b until which the time-dependent ramping process has to be performed in order to obtain single-atom transfer between adjacent wells. The starting configuration depends on the gate voltage under consideration. For $V_\mathrm{g} < 0.4V_0$, we start with a 3:0:3 population at zero bias, which is then transformed into a 2:1:3 state under the increase of V_b and into a 3:1:2 state if instead the bias is ramped into the opposite direction leading to negative V_b. Within $0.4V_0 < V_\mathrm{g} < 0.72V_0$, the initial state corresponds to either a 2:1:3 or a 3:1:2 population, depending on the presence of a tiny positive or negative bias. The final state of the ramping process now depends on the gate voltage. For $V_\mathrm{g} < 0.56V_0$, we obtain the 2:0:4 state (or the 4:0:2 state for negative bias), i.e. the atom in the central well is released to the right (left) well, while for $V_\mathrm{g} > 0.56V_0$ another atom from the left (right) well is pulled into the central well leading to the 1:2:3 (3:2:1) state. A completely analogous situation is realized for gate voltages within $0.72V_0 < V_\mathrm{g} < 1.28V_0$, where we initially encounter a 2:2:2 population—with the only exception that this population obviously does not depend on the presence of a small initial bias.

4.2. Bose–Hubbard theory of the diamonds

The structure and shape of the transition lines in the V_b–V_g parameter space are strongly reminiscent of Coulomb diamonds in electronic quantum dots (see, for example, the very recent work of [34] or the review [28]). This analogy can indeed be straightforwardly worked out in terms of a simple Bose–Hubbard-type model. We take into account for this purpose the three energetically lowest single-particle eigenfunctions (or rather Wannier functions in the case of degeneracies[5]) $\phi_\mathrm{L}(x)$, $\phi_\mathrm{C}(x)$ and $\phi_\mathrm{R}(x)$, corresponding to the particle being

[4] We subdivide for this purpose the time interval δt into 10 000 sub-intervals within which we assume the Hamiltonian to be locally time independent. The propagation within such a sub-interval is performed by the explicit matrix exponentiation.

[5] In the case of degeneracies, $\phi_\mathrm{L}(x)$, $\phi_\mathrm{C}(x)$ and $\phi_\mathrm{R}(x)$ may denote the localized Wannier functions rather than the actual eigenfunctions of the system. The latter would, in the particular case $V_\mathrm{b} = 0$, be given by $\phi_\pm(x) \equiv [\phi_\mathrm{L}(x) \pm \phi_\mathrm{R}(x)]/\sqrt{2}$ and $\phi_\mathrm{C}(x)$.

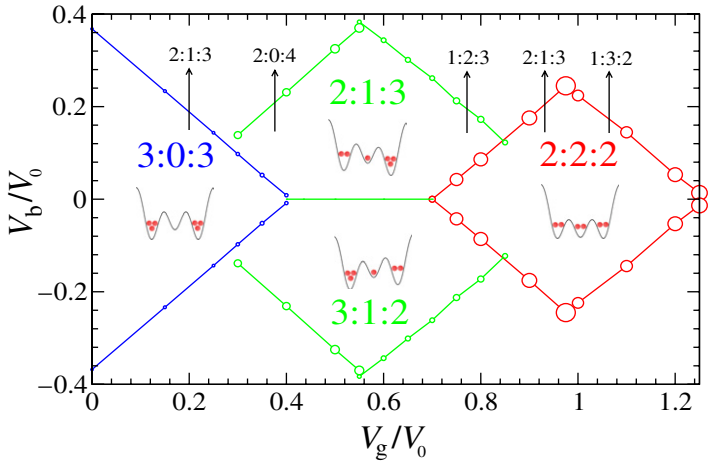

Figure 4. Interaction-blockade diamonds for six atoms in the triple-well potential. Plotted are the minimal (positive and negative) bias voltages V_b until which the time-dependent ramping process (symbolized by the vertical arrows) has to be performed in order to achieve single-atom transfer between adjacent wells. The circles mark the gate voltages for which numerical calculations, based on the computation of the many-body spectrum, were explicitly carried out. The size of the circles indicate the size ΔV_b of the avoided crossings according to equation (21), which is proportional to their level splitting. Note that the avoided crossings become larger with increasing V_g, which corresponds to the fact that the barrier height between the outer wells and the central well is lowered by increasing the gate voltage.

localized in the left, central and right wells. Approximating these single-particle eigenfunctions by normalized Gaussians centered around the minima of the $(-\cos 4kx)$-component of the potential, with a width that corresponds to the local oscillator length $a_{||} = \sqrt{\hbar/(m\omega_{||})}$ with $\omega_{||} \simeq 4k\sqrt{V_0/m}$, the shift of the corresponding single-particle energies due to the presence of finite gate and bias voltages is directly given by V_g and V_b, respectively. More precisely, these energies are approximately given by $E_L = E_0 + V_b$, $E_C = E_1 - V_g$, and $E_R = E_0 - V_b$, with $E_0 \equiv \langle\phi_{L/R}|H_0|\phi_{L/R}\rangle$ and $E_1 \equiv \langle\phi_C|H_0|\phi_C\rangle$, where we define $H_0 \equiv -\frac{\hbar^2}{2m}\frac{\partial^2}{\partial x^2} + V_0(-\cos kx + \cos 2kx - \cos 4kx)$.

The contact interaction $U(x_1 - x_2) = g\delta(x_1 - x_2)$ gives rise to the local interaction energies $E_U^{(L/C/R)} = g\int |\phi_{L/C/R}(x)|^4 dx$ within each well. Using again the above Gaussian ansatz for the single-particle eigenfunctions, these interaction energies are approximately equal to each other and, for $V_0 = 20\hbar^2k^2/m$, given by

$$E_U^{(L/C/R)} \simeq g\sqrt{\frac{m\omega_{||}}{2\pi\hbar}} \simeq 5.37\frac{\hbar^2k^2}{m} \simeq 0.268V_0 \equiv E_U. \tag{4}$$

Neglecting tunnel couplings between the wells, we obtain the Fock states $|N_L, N_C, N_R\rangle$ built upon the single-particle basis (ϕ_L, ϕ_C, ϕ_R) as eigenstates of the many-body system, where N_L, N_C and N_R represent the populations in the left, central and right wells, respectively. The corresponding eigenenergies read

$$E(N_L, N_C, N_R) = E_L(N_L) + E_C(N_C) + E_R(N_R), \tag{5}$$

with

$$E_{\mathrm{L}}(N_{\mathrm{L}}) = N_{\mathrm{L}}\,(E_0 + V_{\mathrm{b}}) + \frac{N_{\mathrm{L}}(N_{\mathrm{L}}-1)}{2}E_U, \tag{6}$$

$$E_{\mathrm{C}}(N_{\mathrm{C}}) = N_{\mathrm{C}}\left(E_1 - V_{\mathrm{g}}\right) + \frac{N_{\mathrm{C}}(N_{\mathrm{C}}-1)}{2}E_U, \tag{7}$$

$$E_{\mathrm{R}}(N_{\mathrm{R}}) = N_{\mathrm{R}}\,(E_0 - V_{\mathrm{b}}) + \frac{N_{\mathrm{R}}(N_{\mathrm{R}}-1)}{2}E_U. \tag{8}$$

Tunneling across the barriers in the potential gives rise to hopping matrix elements between adjacent single-particle states, which are, however, generally much smaller than the above energy scales. Their influence on the many-body eigenstates can therefore be neglected, except for accidental near-degeneracies between the unperturbed energies (5), where they give rise to hybridizations between the involved Fock states $|N_{\mathrm{L}}, N_{\mathrm{C}}, N_{\mathrm{R}}\rangle$. The resulting avoided crossings in the many-body spectrum are most significant if the Fock states that participate at this crossing can be mapped into each other by the exchange of only one atom across one tunneling barrier.

In order to identify the location of these crossings in the parameter space spanned by the gate and bias voltages, we introduce the local particle-addition and -removal energies [16] as

$$\mu^{+}_{\mathrm{L/C/R}}(N_{\mathrm{L/C/R}}) \equiv E_{\mathrm{L/C/R}}(N_{\mathrm{L/C/R}}+1) - E_{\mathrm{L/C/R}}(N_{\mathrm{L/C/R}}), \tag{9}$$

$$\begin{aligned}\mu^{-}_{\mathrm{L/C/R}}(N_{\mathrm{L/C/R}}) &\equiv E_{\mathrm{L/C/R}}(N_{\mathrm{L/C/R}}) - E_{\mathrm{L/C/R}}(N_{\mathrm{L/C/R}}-1)\\ &= \mu^{+}_{\mathrm{L/C/R}}(N_{\mathrm{L/C/R}}-1)\end{aligned} \tag{10}$$

for the left, central and right wells, respectively. With the help of equations (6)–(8), we find

$$\mu^{+}_{\mathrm{L}}(N_{\mathrm{L}}) = E_0 + V_{\mathrm{b}} + N_{\mathrm{L}}E_U, \tag{11}$$

$$\mu^{+}_{\mathrm{C}}(N_{\mathrm{C}}) = E_1 - V_{\mathrm{g}} + N_{\mathrm{C}}E_U, \tag{12}$$

$$\mu^{+}_{\mathrm{R}}(N_{\mathrm{R}}) = E_0 - V_{\mathrm{b}} + N_{\mathrm{R}}E_U. \tag{13}$$

Degeneracies between unperturbed levels that correspond to the populations $N_{\mathrm{L}} : N_{\mathrm{C}} : N_{\mathrm{R}}$ and $N_{\mathrm{L}} \pm 1 : N_{\mathrm{C}} \mp 1 : N_{\mathrm{R}}$ therefore occur if $\mu^{\pm}_{\mathrm{L}}(N_{\mathrm{L}}) = \mu^{\mp}_{\mathrm{C}}(N_{\mathrm{C}})$, which is equivalent to the equation

$$V_{\mathrm{b}} = E_1 - E_0 - V_{\mathrm{g}} + (N_{\mathrm{C}} - N_{\mathrm{L}} \mp 1)E_U. \tag{14}$$

Correspondingly, we find

$$-V_{\mathrm{b}} = E_1 - E_0 - V_{\mathrm{g}} + (N_{\mathrm{C}} - N_{\mathrm{R}} \pm 1)E_U \tag{15}$$

as the equation for the degeneracy between $N_{\mathrm{L}} : N_{\mathrm{C}} : N_{\mathrm{R}}$ and $N_{\mathrm{L}} : N_{\mathrm{C}} \pm 1 : N_{\mathrm{R}} \mp 1$.

With these equations (14) and (15), we can quantitatively predict the location and shape of the 'atom blockade diamonds', i.e. of the transition lines that mark the value of the bias at which single-atom transfer takes place between adjacent wells. This is shown in figure 5 for the case of six particles in the triple-well potential under consideration. We see that the agreement with the numerically computed transition lines in figure 4 is rather good. Taking into account the approximate value (4) for the interaction energy E_U, we can quantitatively reproduce not only the shape but also the size of the diamond structures in figure 4.

There are some important differences to standard Coulomb diamonds in quantum dots. On the one hand, the diamond structures display 'open ends' for both very low and very high gate

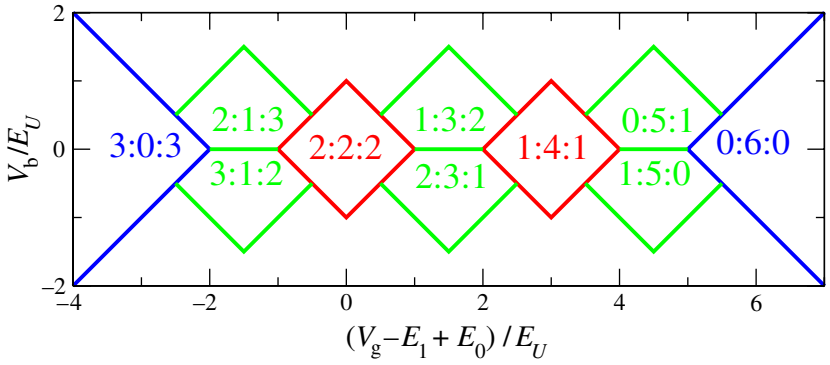

Figure 5. Structure of the interaction-blockade diamonds that result from a simple Bose–Hubbard-type model. Plotted are the predicted transition lines for single-particle transfer between adjacent wells according to equations (14) and (15), assuming the presence of six particles in a triple-well potential with equal on-site interaction energies. The agreement with figure 4 is rather good, taking into account the approximate value $E_U \simeq 0.268V_0$ (4) for the interaction energy.

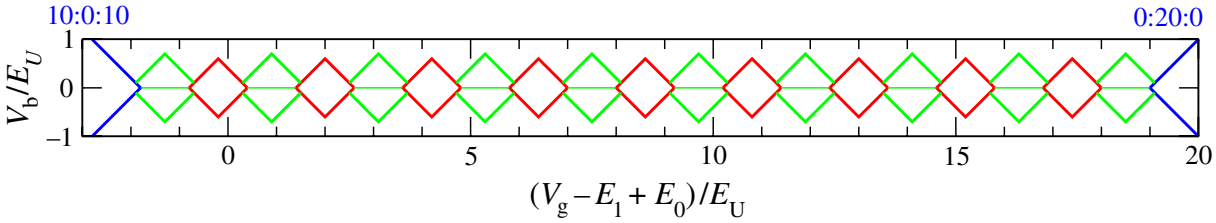

Figure 6. The same as figure 5 for a more mesoscopic situation with 20 particles, where the two outer wells are assumed to be much more shallow and thereby exhibit a lower on-site interaction energy, namely $E_U^{(L/R)} = 0.2E_U^{(C)} \equiv 0.2E_U$, than the central well. This situation resembles much more the standard scenario of Coulomb blockade in electronic quantum dots where the two-particle interaction energy in the leads does not play a role.

voltages, corresponding to an empty quantum dot and to empty reservoirs, respectively. On the other hand, there is significant asymmetry between the diamond structures corresponding to a 'balanced' (with $N_L = N_R$) and an 'unbalanced' population (with $N_L = N_R \pm 1$) in the outer wells. This is a consequence of the finite interaction energy E_U in the reservoirs.

To demonstrate this, we show in figure 6 a more mesoscopic situation involving 20 particles in total, where the two outer wells are assumed to be much more shallow and thereby exhibit a lower on-site interaction energy $E_U^{(L/R)}$ than the central well. This leads to slight modifications of the formulae (14) and (15); we obtain

$$V_b = E_1 - E_0 - V_g + (N_C - 1)E_U^{(C)} - N_L E_U^{(L)}, \tag{16}$$

$$V_b = E_1 - E_0 - V_g + N_C E_U^{(C)} - (N_L - 1)E_U^{(L)}, \tag{17}$$

$$-V_b = E_1 - E_0 - V_g + (N_C - 1)E_U^{(C)} - N_R E_U^{(R)}, \tag{18}$$

$$-V_b = E_1 - E_0 - V_g + N_C E_U^{(C)} - (N_R - 1)E_U^{(R)}. \tag{19}$$

Specifically assuming $E_U^{(\mathrm{L/R})} = 0.2E_U^{(\mathrm{C})}$ in figure 6, the resulting structure of the transition lines for single-particle transfer resembles much more the standard Coulomb diamonds in electronic quantum dots.

Independently of the size of the outer wells, the distance between the edges of the diamonds with balanced populations is, as seen in figures 5 and 6, predicted to be equal to the local interaction energy $E_U^{(\mathrm{C})}$ in the central well. This opens the possibility of extracting the value of this interaction energy from the location of the transition lines of single-atom transfer in the V_g–V_b parameter space. From figure 4 we would approximately infer $E_U^{(\mathrm{C})} \simeq 0.29V_0 \simeq 5.8\hbar^2k^2/m$ from the distance between the corners of the 3:0:3 and 2:2:2 diamonds. This is in fairly good agreement with the numerically computed interaction energy $E_U^{(\mathrm{C})} \simeq 5.1\hbar^2k^2/m$, which is obtained by subtracting twice the lowest single-particle eigenenergy E_1 of the central well from the energy of the lowest two-particle state where both atoms are localized in the central well.

4.3. Energy scales of the avoided crossings

While this simple Bose–Hubbard-type model is capable of reproducing the location of the transition lines for single-atom transfer in the $V_\mathrm{g} - V_\mathrm{b}$ parameter space, it is *not* sufficient to predict the time scales on which the ramping process ought to take place in order to achieve those transitions. As pointed out above, these time scales crucially depend on the sizes of the avoided crossings in the many-body spectrum, which are essentially given by the single-particle hopping matrix elements between different wells. These hopping matrix elements, however, arise from a tunneling process across the barriers that separate the wells from each other. They are therefore sensitively dependent on the effective *height* of the barriers with respect to the particle-addition or -removal energies under consideration, which in turn is appreciably modified under variation of the bias or gate voltages.

Specifically, we find that an increase in the gate voltage, corresponding to 'pulling down' the central well with respect to the outer ones, generally gives rise to a significant enlargement of the avoided crossings between different many-body levels. This is illustrated in figure 4 in which the size of the circles indicate the extent ΔV_b of the avoided crossings between the states under consideration in bias voltage space. More precisely, if we describe the general dependence of the level splitting between two near-degenerate states on the bias voltage by

$$\Delta E(V_\mathrm{b}) = \Delta E\sqrt{1 + \left(\nu(V_\mathrm{b} - V_\mathrm{b}^{(\mathrm{c})})/\Delta E\right)^2}, \tag{20}$$

where $\Delta E \equiv \Delta E(V_\mathrm{b}^{(\mathrm{c})})$ and $V_\mathrm{b}^{(\mathrm{c})}$ denote the splitting and bias voltages, respectively, at the crossing point and ν represents the (nearly integer) difference between the variations in the unperturbed levels with V_b far away from the anticrossing. We define

$$\Delta V_\mathrm{b} \equiv 2\Delta E/\nu \tag{21}$$

as the maximal extent of the avoided crossing in bias voltage space. For anticrossings that correspond to single-atom transfer between adjacent wells, we have $\nu \simeq 1$ and therefore $\Delta V_\mathrm{b} \simeq 2\Delta E$.

Table 1 lists the level splittings at the avoided crossings that the system undergoes during the time-dependent ramping process, for the gate voltages $V_\mathrm{g} = 0.25V_0$, $0.5V_0$ and $1.0V_0$. For each of those gate voltages, the first one of the encountered anticrossings corresponds to a

Table 1. Level splittings (in units of $\hbar^2 k^2/m$) of the first two avoided crossings that are encountered during the ramping process of the bias voltage, for $V_g = 0.25V_0$, $0.5V_0$ and $1.0V_0$.

		First crossing			Second crossing		
Gate voltage	Initial state	Bias voltage	Crossing state	Level splitting	Bias voltage	Crossing state	Level splitting
$0.25V_0$	3:0:3	$0.117V_0$	2:0:4	0.0015	$0.143V_0$	2:1:3	0.069
$0.5V_0$	2:1:3	$0.248V_0$	1:1:4	0.019	$0.325V_0$	2:0:4	0.16
$1.0V_0$	2:2:2	$0.128V_0$	1:2:3	0.047	$0.221V_0$	1:3:2	0.22

double-barrier tunneling process of an atom that is directly transferred from the left to the right wells. Correspondingly, the associated anticrossing is much smaller than the one of the second anticrossing describing a single-barrier tunneling process. This particularly implies that it is, for all of these cases, possible to define, according to the Landau–Zener formula (3), a reasonably large range of speeds s for the ramping process $V_b(t) = st$, such that the system undergoes a diabatic transition across the first anticrossing and an adiabatic transition at the second anticrossing. However, comparing the level splittings for *different* values of V_g, we realize that this range of speeds will depend on the particular gate voltage under consideration and that it is hardly possible to choose one 'universal' ramping speed with which the desired single-atom transfer can be carried out for all gate voltages. This is another manifestation of the microscopic nature of this transport system.

A relevant question is whether the interaction-blockade phenomena discussed here are also observable for lower effective 1D interaction strengths g, i.e. in the presence of a weaker transverse confinement of the waveguide. Figure 5 seems to affirm this, as the structure of the diamonds does not explicitly depend on the interaction strength, except for the scaling of the horizontal and vertical axes that is directly proportional to g. However, the size and extent of the relevant avoided crossings, on the other hand, do, in lowest order, *not* scale with g, as they are essentially given by the single-particle hopping matrix element between adjacent sites. This implies that decreasing the effective interaction strength g, e.g. by a factor of ten, will, in lowest order, give rise to the same relative location of the transition lines in figure 4, with the V_g and V_b axes scaled down by a factor of ten, while the 'uncertainty' of the transition lines, given by the extent of the corresponding avoided crossings and represented by the size of the circles in figure 4, will be increased by a factor of ten.

The interaction-blockade diamonds ultimately become unobservable if the on-site interaction energy is of the same order as the tunneling matrix element between adjacent sites. In that case, *collective* instead of single-atom transfer processes begin to take place. For the ground state populations in figure 2, this would imply that the staircase structure of the left- and right-well populations would shrink down to a very small interval of V_b around $V_b = 0$, with the individual steps becoming smeared out, leading to a nearly direct transition from a 6:0:0 to a 0:0:6 population. Similarly, the diamond structures would become smeared out in figure 4, and a tuning of the gate voltage would, at zero bias $V_b = 0$, lead to a nearly direct transition between a 3:0:3 and a 0:6:0 population, via intermediate states that cannot be uniquely associated with integer populations in the left, central or right wells. This underlines again

the obvious requirement that the transport processes discussed here must be performed in the 'Mott-insulator regime' of strong on-site interaction and weak tunneling within the triple-well potential.

5. Discussion and conclusion

In summary, we studied a microscopic analogue of source–drain transport with ultracold bosonic atoms in a triple-well potential. The latter is considered to be realized by optical triple-well lattices in analogy with the experiments of [15, 17], which are initially loaded with a well-defined number of atoms per site. We now propose performing a time-dependent tilt of these triple-well potentials until a given maximal bias, followed by measuring the resulting populations in the individual wells. This process can be repeated for various values of a 'gate voltage', which lowers the level of the central well with respect to the outer ones. Diamond structures are obtained for the transition lines that mark the necessary values for the bias in order to achieve single-atom transfer between adjacent wells, when being plotted as a function of that gate voltage. These diamonds can be used to infer the local interaction energy in the central well.

There are striking similarities with Coulomb diamonds in electronic quantum dots, but also some important differences from the latter, which mainly arise due to the microscopic nature of the 'reservoirs' in the outer two wells. Most characteristically, 'transport' is manifested not by a continuous flow of particles across the quantum dot but rather by the transfer of a single atom from one well to another. This transport process is, in general, not 'completed' insofar as the atom when, e.g., being transferred from the left to the central well will not directly go on to the right well, due to the mismatch of the corresponding particle-addition and -removal energies. Close to the corners of the diamond structures (e.g. at $V_g \simeq 0.3V_0$, see figure 4), this latter task can eventually be achieved by further increasing the bias. In general, however, more complicated ramping processes, involving also a time-dependent variation of the gate voltage, would be required for that purpose. This is clearly a consequence of the finite two-body interaction energy in the reservoirs, which also leads to a striking asymmetry between diamond structures corresponding to balanced and unbalanced populations in the outer wells.

The microscopic transport scheme that we investigated here can also be applied to more complex atomic gases involving, e.g., several spin components and/or long-range dipolar interaction. This will open various possibilities for the exploration of the interplay of interaction and transport in an experimentally feasible context. Our findings should, moreover, be relevant for cyclic processes [35], as well as for the evaluation of the feasibility of atomtronic scenarios and atomic transistors [13, 36, 37], and they might provide valuable insight for the design of logical operations with single atoms.

Acknowledgments

We thank I Bloch, I Březinová, K Capelle, G Kavoulakis, M Oberthaler, C Pethick, M Rontani, A Wacker and S Zöllner for useful discussions. This work was financially supported by the Swedish Research Council and the Swedish Foundation for Strategic Research. The collaboration is part of the NordForsk Nordic network *Coherent Quantum Gases—From Cold Atoms to Condensed Matter*.

References

[1] Morsch O and Oberthaler M 2006 *Rev. Mod. Phys.* **78** 179
[2] Folman R, Krüger P, Cassettari D, Hessmo B, Maier T and Schmiedmayer J 2000 *Phys. Rev. Lett.* **84** 4749
[3] Fortágh J and Zimmermann C 2007 *Rev. Mod. Phys.* **79** 235
[4] Leboeuf P and Pavloff N 2001 *Phys. Rev.* A **64** 033602
[5] Leboeuf P, Pavloff N and Sinha S 2003 *Phys. Rev.* A **68** 063608
[6] Carusotto I and La Rocca G C 2000 *Phys. Rev. Lett.* **84** 399
[7] Carusotto I 2001 *Phys. Rev.* A **63** 023610
[8] Paul T, Richter K and Schlagheck P 2005 *Phys. Rev. Lett.* **94** 020404
[9] Paul T, Hartung M, Richter K and Schlagheck P 2007 *Phys. Rev.* A **76** 063605
[10] Rapedius K, Witthaut D and Korsch H J 2006 *Phys. Rev.* A **73** 033608
[11] Guerin W, Riou J-F, Gaebler J P, Josse V, Bouyer P and Aspect A 2006 *Phys. Rev. Lett.* **97** 200402
[12] Couvert A, Jeppesen M, Kawalec T, Reinaudi G, Mathevet R and Guéry-Odelin D 2008 *Europhys. Lett.* **83** 50001
[13] Stickney J A, Anderson D Z and Zozulya A A 2007 *Phys. Rev.* A **75** 013608
[14] Campey T, Vale C J, Davis M J, Heckenberg N R, Rubinsztein-Dunlop H, Kraft S, Zimmermann C and Fortágh J 2006 *Phys. Rev.* A **74** 043612
[15] Fölling S, Trotzky S, Cheinet P, Feld M, Saers R, Widera A, Müller T and Bloch I 2007 *Nature* **448** 1029
[16] Capelle K, Borgh M, Kärkkäinen K and Reimann S M 2007 *Phys. Rev. Lett.* **99** 010402
[17] Cheinet P, Trotzky S, Feld M, Schnorrberger U, Moreno-Cardoner M, Fölling S and Bloch I 2008 *Phys. Rev. Lett.* **101** 090404
[18] Dounas-Frazer D R, Hermundstad A M and Carr L D 2007 *Phys. Rev. Lett.* **99** 200402
[19] Zöllner S, Meyer H D and Schmelcher P 2007 *Phys. Rev.* A **75** 043608
[20] Zöllner S, Meyer H P and Schmelcher P 2008 *Phys. Rev.* A **78** 013621
[21] Zöllner S, Meyer H D and Schmelcher P 2008 *Phys. Rev. Lett.* **100** 040401
[22] Averin D V, Bergeman T, Hosur P R and Bruder C 2008 *Phys. Rev.* A **78** 031601
[23] Lambe J and Jaklevic R C 1969 *Phys. Rev. Lett.* **22** 1371
[24] Averin D V and Likharev K K 1996 *J. Low Temp. Phys.* **62** 345
[25] Averin D V and Likharev K K 1991 *Mesoscopic Phenomena in Solids* ed B I Altshuler, P A Lee and R A Webb (Amsterdam: Elsevier)
[26] Grabert H and Devoret M H (ed) 1991 *Single Charge Tunneling* (New York: Plenum)
[27] Meir Y, Wingreen N S and Lee P A 1991 *Phys. Rev. Lett.* **66** 3048
[28] Reimann S M and Manninen M 2002 *Rev. Mod. Phys.* **74** 1283
[29] Kierig E, Schnorrberger U, Schietinger A, Tomkovic J and Oberthaler M K 2008 *Phys. Rev. Lett.* **100** 190405
[30] Olshanii M 1998 *Phys. Rev. Lett.* **81** 938
[31] Lanczos C 1950 *J. Res. Natl Bur. Stand.* **45** 255
[32] Zener C 1932 *Proc. R. Soc.* A **137** 696
[33] Park T J and Light J C 1986 *J. Chem. Phys.* **85** 5870
[34] Fuhrer A, Fröberg L E, Pedersen J N, Larsson M W, Wacker A, Pistol M-E and Samuelson L 2007 *Nano Lett.* **7** 243
[35] Hiller M, Kottos T and Cohen D 2008 *Europhys. Lett.* **82** 40006
[36] Seaman B T, Krämer M, Anderson D Z and Holland M J 2007 *Phys. Rev.* A **75** 023615
[37] Pepino R A, Cooper J, Anderson D Z and Holland M J 2009 *Phys. Rev. Lett.* **103** 140405